

Article

## Mechanical Diaphragm Structure Design of a MEMS-Based Piezoresistive Pressure Sensor for Sensitivity and Linearity Enhancement

Phongsakorn Thawornsathit<sup>1,a</sup>, Ekachai Juntasaro<sup>1,b,\*</sup>, Hwanjit Rattanasonti<sup>2,c</sup>,  
Putapon Pengpad<sup>2,d</sup>, Karoon Saejok<sup>2,e</sup>, Chana Leepattarapongpan<sup>2,f</sup>,  
Ekalak Chaowicharat<sup>2,g</sup>, and Wutthinan Jeamsaksiri<sup>2,h</sup>

<sup>1</sup> Mechanical Engineering Simulation and Design Group, The Sirindhorn International Thai-German Graduate School of Engineering (TGGS), King Mongkut's University of Technology North Bangkok (KMUTNB), Bangkok 10800, Thailand

<sup>2</sup> Thai Microelectronics Center (TMEC), National Electronics and Computer Technology Center, National Science and Technology Development Agency, Chachoengsao 24000, Thailand

E-mail: <sup>a</sup>s6209091960016@email.kmutnb.ac.th, <sup>b,\*</sup>ekachai.j@tggs.kmutnb.ac.th (Corresponding author),

<sup>c</sup>hwanjit.rattanasonti@nectec.or.th, <sup>d</sup>putapon.pengpad@nectec.or.th, <sup>e</sup>karoon.saejok@nectec.or.th,

<sup>f</sup>chana.leepattarapongpan@nectec.or.th, <sup>g</sup>ekalak.chaowicharat@nectec.or.th,

<sup>h</sup>wutthinan.jeamsaksiri@nectec.or.th

**Abstract.** An improved design of the micro-electromechanical system (MEMS) piezoresistive pressure sensor with a combination of a petal edge, a beam, a peninsula, three cross beams and a center boss is proposed in this work for an operating range of low pressure in order to improve the sensor performance, i.e. the sensitivity and the linearity. The finite element method (FEM) is utilized to predict the stress and the deflection of the MEMS piezoresistive pressure sensor under the applied pressure of 1-5 kPa. The functional forms of the longitudinal stress, the transverse stress and the deflection are formulated by using the power law and then are used to optimize the geometry of the proposed design. The simulation results show that the proposed design is able to produce the high sensitivity up to 34 mV/kPa with the low nonlinearity of 0.11% full-scale span (FSS). The nonlinearity error is lowered by the proposed design of the peninsula, three cross beams and the center boss. The sensitivity is enhanced by increasing the petal edge width. The sensor performance of the proposed design is also compared to that of the previous design in the literature. The comparison reveals that the proposed design can perform better than the previous one.

**Keywords:** MEMS, piezoresistive pressure sensor, finite element method, sensitivity, linearity.

ENGINEERING JOURNAL Volume 26 Issue 5

Received 31 December 2021

Accepted 10 May 2022

Published 31 May 2022

Online at <https://engj.org/>

DOI:10.4186/ej.2022.26.5.43

## 1. Introduction

Micro-electromechanical system (MEMS) pressure sensor is one of the most widely used devices in MEMS industry [1-3]. It is attractive because it is small in size, requires a low power supply, provides high efficiency/performance and is suitable for mass production [2-3]. Based on sensing principles, there are mainly four types of MEMS pressure sensor that are widely used in the community: capacitive, resonant, optical and piezoresistive sensors [1]. Each sensor type has its own advantage and disadvantage. The capacitive pressure sensor has the advantage of high precision and accuracy but the applied pressure range is limited due to the nonlinearity output and the strict environmental requirement [4]. The resonant pressure sensor has the advantage of its long-term stability [5]. It can directly output digital signals with high precision and accuracy, high sensitivity and low temperature sensitivity but it needs high-quality materials for vibrator and a complex fabrication process leading to high cost and a time-consuming fabrication process [1, 5, 6]. The optical pressure sensor has high stability and accuracy without any problem in electromagnetic interface (EMI) but it often suffers from temperature sensitivity and has strict installation limit [1, 7, 8]. The piezoresistive pressure sensor has a smaller size and high performance [2, 9, 10, 11] so that it has been most widely used in various applications such as automobile, aerospace [9, 12], biomedical equipment [3, 9] and process control units in petrochemical industry [8]. As reported in [13, 14], the MEMS piezoresistive pressure sensor is highly needed in the pressure sensor market. The main factors considered for designing the MEMS piezoresistive pressure sensor are high accuracy, high pressure sensitivity, high linearity and low temperature sensitivity [15]. To improve the performance of piezoresistive pressure sensors, there are three possible approaches to achieve this goal: application of new material for the sensing elements, design of new electrical circuit and design of new diaphragm structure. First approach, the piezoresistive effect on nanotubes was studied and applied to the piezoresistor, where the pressure sensitivity was significantly increased [16, 17]. Second approach, instead of the Wheatstone bridge, the PDA-NFL circuit was used to help increase the sensitivity and reduce the sensor size [18, 19]. Third approach, several research groups attempted to improve the sensitivity and the linearity by changing diaphragm geometry. Figure 1 shows the development of the diaphragm structure from 1993 to 2018. Sandmaier and Kuhl (1993) [20] proposed a square diaphragm with a rectangular central boss that significantly improved the linearity and the sensitivity. Tian et al. (2010) [4] designed a cross-beam structure on the diaphragm that improved both the sensitivity and the linearity compared to the flat diaphragm but their design gained the low sensitivity with the high nonlinearity error, i.e. 7.359 mV/kPa and 0.19%

FSS respectively. Huang and Zhang (2014) [21] proposed a peninsula-structure diaphragm that highly enhanced the sensitivity compared to the cross-beam one but the higher nonlinearity error was obtained in return, i.e. 0.36% FSS. Guan et al. (2017) [22] proposed a shuriken-structure diaphragm that gained the sensitivity 28% higher and reduced the nonlinearity error 100% lower compared to the peninsula-structure one. Zhu et al. (2017) [23] designed a diaphragm structure by using the topology optimization in order to obtain the diaphragm geometry that was able to produce high stress at the piezoresistor placement with low deflection at the center of the diaphragm. Tran et al. (2018a) [24] proposed a diaphragm structure that comprised cross-beam and peninsula structures. Although the sensitivity was found to be 6.5% lower than that of the peninsula-structure diaphragm, the nonlinearity error was decreased over 50%. In the same year, Tran et al. (2018b) [25] proposed a petal-edge diaphragm combined with a cross beam, a peninsula structure and a center boss that significantly improved the sensitivity without the negative effect on the linearity compared to the diaphragm structure of Tran et al. (2018a) [24]. The temperature sensitivity was decreased by using the base resistance of a MOSFET as the piezoresistor in the Wheatstone bridge circuit [19, 26].

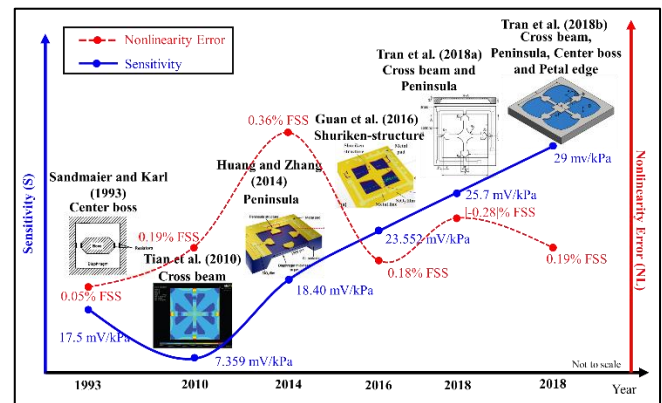


Fig. 1. Development of the diaphragm structure from 1993 to 2018.

To improve the performance of the MEMS piezoresistive pressure sensor, design of the diaphragm geometry is considered because it can be done routinely by simulation to improve both sensitivity and linearity. In this paper, the MEMS piezoresistive pressure sensor of Tran et al. (2018b) [25] is further developed to improve the sensitivity and the linearity. A combination of a petal edge, a beam, a peninsula, three cross beam and a center boss is carefully designed together for sensor improvement. The finite element method (FEM) is used to calculate the stress and the deflection in order to evaluate the performance of the proposed MEMS piezoresistive pressure sensor under the applied pressure of 1-5 kPa. The variations of the longitudinal stress, the transverse stress and the deflection with twelve geometric

parameters are determined and formulated by using the power law in order to create their functional forms. Then, the functional forms of the longitudinal stress, the transverse stress and the deflection are used to optimize the presently designed MEMS piezoresistive pressure sensor. Finally, the sensitivity and the nonlinearity error of this optimal design are compared to those of Tran et al. (2018b) [25].

## 2. Methodology

### 2.1. Piezoresistivity

Piezoresistivity is the material property that indicates the electrical resistivity change when strain occurs in material. When the material used is highly piezoresistive, the sensor will thus be highly sensitive to the applied pressure. Silicon is one of the materials that is highly piezoresistive and therefore is widely used to fabricate many types of MEMS sensor, including MEMS piezoresistive pressure sensor, by using micro-machining techniques. Because of the complicated fabrication process and the difficulty with mechanical testing, it leads to the difficulty with design of sensor structure to achieve high efficiency. The finite element method (FEM) is used together with the mathematical model of silicon piezoresistivity to design the MEMS piezoresistive pressure sensor in several previous works [4, 21 - 26].

Johns (2006) [27] reported that the change in the silicon resistivity per unit of resistivity is directly proportional to the stress and the piezoresistive coefficient is the proportionality constant as follows:

$$\frac{1}{\rho} \begin{pmatrix} \Delta\rho_1 \\ \Delta\rho_2 \\ \Delta\rho_3 \\ \Delta\rho_4 \\ \Delta\rho_5 \\ \Delta\rho_6 \end{pmatrix} = \begin{bmatrix} \pi_{11} & \pi_{12} & \pi_{12} & 0 & 0 & 0 \\ \pi_{12} & \pi_{11} & \pi_{12} & 0 & 0 & 0 \\ \pi_{12} & \pi_{12} & \pi_{11} & 0 & 0 & 0 \\ 0 & 0 & 0 & \pi_{44} & 0 & 0 \\ 0 & 0 & 0 & 0 & \pi_{44} & 0 \\ 0 & 0 & 0 & 0 & 0 & \pi_{44} \end{bmatrix} \begin{bmatrix} \sigma_1 \\ \sigma_2 \\ \sigma_3 \\ \sigma_4 \\ \sigma_5 \\ \sigma_6 \end{bmatrix} \quad (1)$$

where  $\rho$ ,  $\pi$  and  $\sigma$  are the silicon resistivity, the piezoresistive coefficient and the stress respectively. The resistance change per unit of resistance becomes a function of stress that occurs on the piezoresistor [28] as follows:

$$\frac{\Delta R}{R} = \sigma_l \pi_l - \sigma_t \pi_t \quad (2)$$

where the subscript  $l$  denotes the direction of stress that is parallel to the current direction which is called "longitudinal stress" and the subscript  $t$  denotes the direction of stress that is perpendicular to the current direction which is called "transverse stress". The direction of the crystallographic plane of silicon on the piezoresistor affects the calculations of  $\pi_l$  and  $\pi_t$  which depend on the strain direction as shown by Messina et al. (2018) [28] in Table 1.

Table 1. The formular of longitudinal and transverse piezoresistive coefficient for the difference in the configurations of the piezoresistor.

Direction of Strain	Direction of Current	Configuration	Formula
<100>	<100>	$\pi_l$	$\pi_{11}$
<100>	<010>	$\pi_t$	$\pi_{12}$
<110>	<110>	$\pi_l$	$(\pi_{11} + \pi_{12} + \pi_{44}) / 2$
<110>	<110>	$\pi_t$	$(\pi_{11} + \pi_{12} - \pi_{44}) / 2$
<111>	<111>	$\pi_l$	$(\pi_{11} + 2\pi_{12} + \pi_{44}) / 2$

The values of piezoresistive coefficients ( $\pi_{11}$ ,  $\pi_{12}$ ,  $\pi_{44}$ ) of silicon p-type and n-type are provided in Table 2 [29].

Table 2. Values of piezoresistive coefficients of single-crystal silicon.

Piezoresistive Coefficient	n-type (Pa <sup>-1</sup> )	p-type (Pa <sup>-1</sup> )
$\pi_{11}$	-102.2×10 <sup>-11</sup>	6.6×10 <sup>-11</sup>
$\pi_{12}$	53.4×10 <sup>-11</sup>	-1.1×10 <sup>-11</sup>
$\pi_{44}$	-13.6×10 <sup>-11</sup>	138.1×10 <sup>-11</sup>

### 2.2. Working Principle of the Piezoresistive Pressure Sensor

The flexible layer of the MEMS piezoresistive pressure sensor is a diaphragm. When the pressure is applied, the diaphragm will deform and the piezoresistors that are arranged in a Wheatstone bridge will be subjected to the longitudinal stress and the transverse stress causing the change in the piezoresistor resistance because of the piezoresistive effect. To evaluate the performance of the MEMS piezoresistive pressure sensor, there are two important parameters used: the sensitivity ( $S$ ) and the nonlinearity error ( $NL$ ).

Figure 2 shows the variables used to calculate the sensitivity and the nonlinearity error of the MEMS piezoresistive pressure sensor. The sensitivity is defined as the change in the output signal due to the applied pressure and can be calculated by using the following expression [25]:

$$S = \frac{V_{out, P_{max}} - V_{out, P_{min}}}{P_{max} - P_{min}} = \frac{V_{FS}}{P_{max} - P_{min}} \quad (3)$$

where  $P_{max}$  and  $P_{min}$  are the maximum and minimum applied pressures in the range of pressure measurements respectively.  $V_{out, P_{max}}$  and  $V_{out, P_{min}}$  are the measured output voltages due to  $P_{max}$  and  $P_{min}$  respectively.  $V_{FS}$  is the full-scale output. The nonlinearity error can be calculated by using the following expression [25]:

$$NL_i = 100\% \times \left[ (V_{out, P_i} - V_{out, P_{min}}) - \left( \frac{V_{FS}}{P_{max} - P_{min}} \right) P_i \right] / V_{FS} = 100\% \times \frac{\Delta V_i}{V_{FS}} \quad (4)$$

where the subscript  $i$  denotes the value of the parameter at the location of interest.

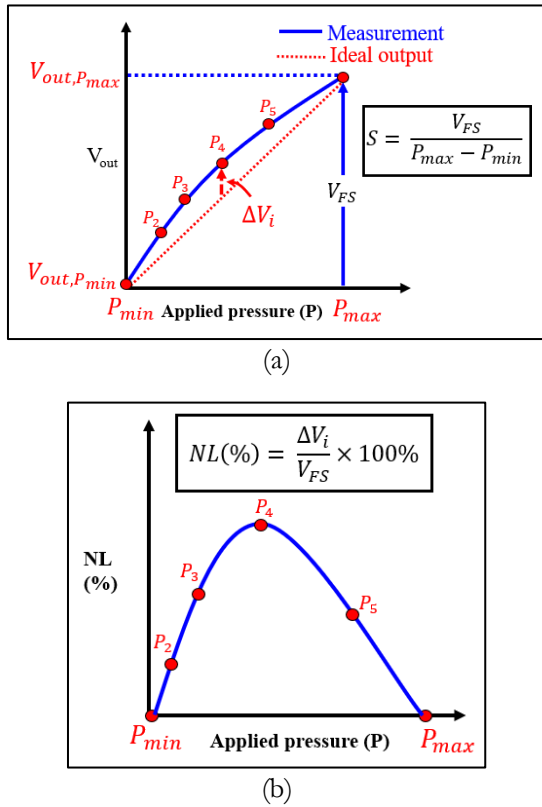


Fig. 2. Variables used to calculate the sensor performance: sensitivity (a) and the nonlinearity error (b) of the MEMS piezoresistive pressure sensor.

In this study, the full Wheatstone bridge is used in the electrical circuit of the proposed MEMS piezoresistive pressure sensor. The Wheatstone bridge is composed of two longitudinal piezoresistors ( $R_1$  and  $R_3$ ) and two transverse piezoresistors ( $R_2$  and  $R_4$ ) where the fractional resistance changes of two longitudinal piezoresistors are equal ( $\Delta R_1 / R_1 = \Delta R_3 / R_3$ ) and the fractional resistance changes of two transverse piezoresistors are equal ( $\Delta R_2 / R_2 = \Delta R_4 / R_4$ ). Therefore, the output voltage can be described as [25]

$$V_{out} = \left\{ \frac{(\Delta R_1 / R_1) - (\Delta R_2 / R_2)}{2 + (\Delta R_1 / R_1) + (\Delta R_2 / R_2)} \right\} V_{in} \quad (5)$$

where  $V_{in}$  is the input voltage. On the n-type (100)-oriented plane of a silicon layer, the p-type piezoresistors are fabricated in the  $\langle 110 \rangle$  direction.  $(\Delta R_1 / R_1)$  and  $(\Delta R_2 / R_2)$  can be expressed, according to Eq. (2), as

$$\frac{\Delta R}{R} = \frac{\pi_{44}(\sigma_l - \sigma_t)}{2} \quad (6)$$

where  $\pi_{11}$  and  $\pi_{12}$  are neglected due to their very low value when compared to  $\pi_{44}$  as shown in Table 2. The

nonlinearity error of the MEMS piezoresistive pressure sensor is used to evaluate the accuracy of the MEMS piezoresistive pressure sensor.

### 2.3. MEMS Piezoresistive Pressure Sensor Design

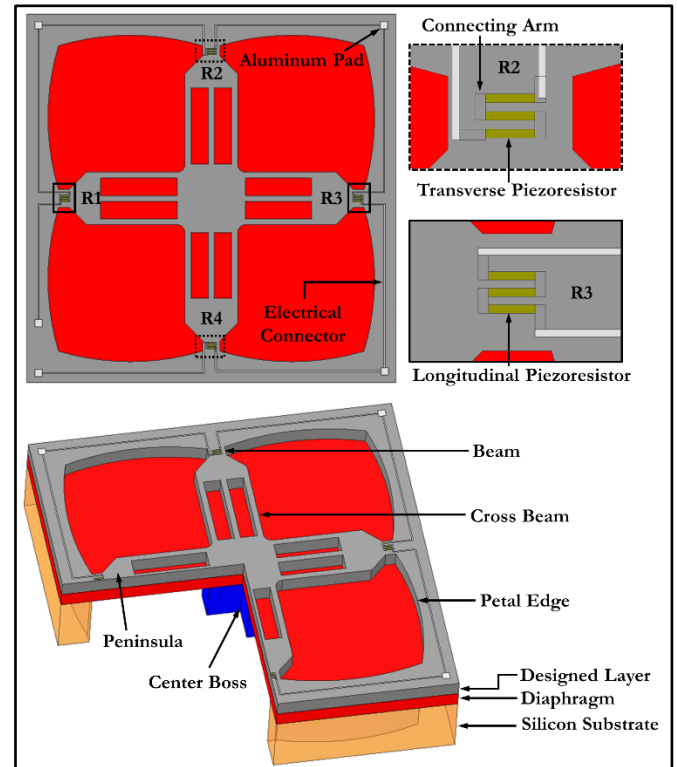


Fig. 3. MEMS piezoresistive pressure sensor designed and proposed in this work. (not to scale).

Figure 3 shows the proposed MEMS piezoresistive pressure sensor designed in this study. There are three main layers designed to improve the sensitivity and the linearity: the designed layer, the diaphragm and the center boss. The designed layer comprises four edges and four bars. Each designed layer edge is divided into two petal edges, according to Tran et al. (2018b) [25], because the petal edge can help induce the longitudinal stress higher on the top surface of the beam leading to higher sensitivity. Four bars are connected to each other at the center of the designed layer. Each bar consists of three specific structures: one beam, one peninsula and three cross beams. The beam that is located in the middle of two petal edges can generate high longitudinal stress on its top surface. Therefore, both the longitudinal piezoresistors ( $R_1$  and  $R_3$ ) and the transverse piezoresistors ( $R_2$  and  $R_4$ ) are placed on the top surface of the beam in order to gain increasing sensitivity. Moreover, the beam can reduce the deflection by increasing the diaphragm stiffness leading to lower nonlinearity error. The peninsula is placed between the beam and the cross beams. The peninsula can increase the sensitivity with slightly decreasing nonlinearity error.

Table 3. List of case studies for the proposed MEMS piezoresistive pressure sensor.

	Parameters												
Unit	$\mu\text{m}$											degree	kPa
Case No.	<i>a</i>	<i>b</i>	<i>c</i>	<i>d</i>	<i>e</i>	<i>f</i>	<i>g</i>	<i>h</i>	<i>i</i>	<i>j</i>	<i>k</i>	$\theta$	<i>P</i>
1	100	2900	500	100	400	650	170	57	12	16	200	45	1-5
2	125	2900	500	100	400	650	170	57	12	16	200	45	1-5
3	150	2900	500	100	400	650	170	57	12	16	200	45	1-5
4	175	2900	500	100	400	650	170	57	12	16	200	45	1-5
5	100	3200	500	100	400	650	170	57	12	16	200	45	1-5
6	100	3500	500	100	400	650	170	57	12	16	200	45	1-5
7	100	3800	500	100	400	650	170	57	12	16	200	45	1-5
8	100	2900	250	100	400	650	170	57	12	16	200	45	1-5
9	100	2900	375	100	400	650	170	57	12	16	200	45	1-5
10	100	2900	625	100	400	650	170	57	12	16	200	45	1-5
11	100	2900	500	125	400	650	170	57	12	16	200	45	1-5
12	100	2900	500	150	400	650	170	57	12	16	200	45	1-5
13	100	2900	500	175	400	650	170	57	12	16	200	45	1-5
14	100	2900	500	100	525	650	170	57	12	16	200	45	1-5
15	100	2900	500	100	650	650	170	57	12	16	200	45	1-5
16	100	2900	500	100	775	650	170	57	12	16	200	45	1-5
17	100	2900	500	100	400	810	170	57	12	16	200	45	1-5
18	100	2900	500	100	400	975	170	57	12	16	200	45	1-5
19	100	2900	500	100	400	1140	170	57	12	16	200	45	1-5
20	100	2900	500	100	400	650	210	57	12	16	200	45	1-5
21	100	2900	500	100	400	650	250	57	12	16	200	45	1-5
22	100	2900	500	100	400	650	290	57	12	16	200	45	1-5
23	100	2900	500	100	400	650	170	70	12	16	200	45	1-5
24	100	2900	500	100	400	650	170	85	12	16	200	45	1-5
25	100	2900	500	100	400	650	170	100	12	16	200	45	1-5
26	100	2900	500	100	400	650	170	57	13	16	200	45	1-5
27	100	2900	500	100	400	650	170	57	15	16	200	45	1-5
28	100	2900	500	100	400	650	170	57	16	16	200	45	1-5
29	100	2900	500	100	400	650	170	57	12	18	200	45	1-5
30	100	2900	500	100	400	650	170	57	12	24	200	45	1-5
31	100	2900	500	100	400	650	170	57	12	28	200	45	1-5
32	100	2900	500	100	400	650	170	57	12	16	250	45	1-5
33	100	2900	500	100	400	650	170	57	12	16	300	45	1-5
34	100	2900	500	100	400	650	170	57	12	16	350	45	1-5
35	100	2900	500	100	400	650	170	57	12	16	200	30	1-5
36	100	2900	500	100	400	650	170	57	12	16	200	60	1-5

Three cross beams are proposed in this study, instead of one cross beam proposed by Zhu et al. (2017) [23], because the linearity can be significantly improved without the negative effect on the sensitivity when one cross beam is divided equally into three cross beams. The diaphragm is placed between the designed layer and the n-type silicon substrate. The cavity is an empty space below the diaphragm and is enclosed by the substrate. Inside the cavity, the center boss is fixed under the center of the diaphragm, which can help increase the diaphragm stiffness leading to lower nonlinearity error.

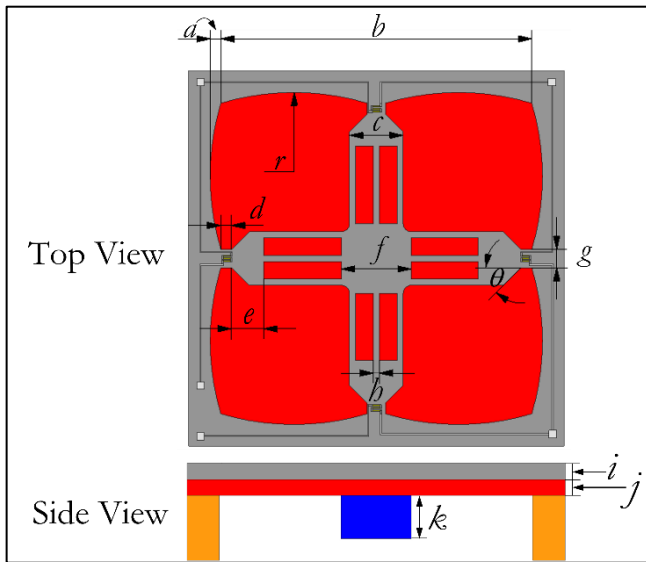


Fig. 4. Geometric parameters of the proposed MEMS piezoresistive pressure sensor: Grey is the designed layer, Red is the diaphragm, Blue is the center boss, Gold is the piezoresistor and Orange is the substrate. (not to scale).

In Fig. 4, there are twelve geometric parameters that are necessary for formulating the functional forms of the maximum longitudinal stress ( $\sigma_l$ ), the maximum transverse stress ( $\sigma_t$ ) and the maximum diaphragm deflection ( $\delta$ ) of this MEMS piezoresistive pressure sensor: the petal edge width ( $a$ ), the diaphragm width ( $b$ ), the peninsula width ( $c$ ), the beam length ( $d$ ), the peninsula length ( $e$ ), the center boss width ( $f$ ), the beam width ( $g$ ), the cross beam width ( $h$ ), the designed layer thickness ( $i$ ), the diaphragm thickness ( $j$ ), the center boss thickness ( $k$ ) and the inclined angle between the beam and the peninsula ( $\theta$ ) where the radius of the petal edge ( $r$ ) depends on  $a$ ,  $b$  and  $g$ , and can be expressed as  $r = \left\{ a^2 + \left[ (b-g)/4 \right]^2 \right\} / 2a$ .

The functional forms of  $\sigma_l$ ,  $\sigma_t$  and  $\delta$  can be determined by applying the power law to each geometric parameter as follows:

$$\sigma_l = N_1 \cdot a^{\alpha_1} \cdot b^{\alpha_2} \cdot c^{\alpha_3} \cdot d^{\alpha_4} \cdot e^{\alpha_5} \cdot f^{\alpha_6} \cdot g^{\alpha_7} \cdot h^{\alpha_8} \cdot i^{\alpha_9} \cdot j^{\alpha_{10}} \cdot k^{\alpha_{11}} \cdot \theta^{\alpha_{12}} \cdot p^{\alpha_{13}} \quad (7)$$

$$\sigma_t = N_2 \cdot a^{\beta_1} \cdot b^{\beta_2} \cdot c^{\beta_3} \cdot d^{\beta_4} \cdot e^{\beta_5} \cdot f^{\beta_6} \cdot g^{\beta_7} \cdot h^{\beta_8} \cdot i^{\beta_9} \cdot j^{\beta_{10}} \cdot k^{\beta_{11}} \cdot \theta^{\beta_{12}} \cdot p^{\beta_{13}} \quad (8)$$

$$\delta = N_3 \cdot a^{\gamma_1} \cdot b^{\gamma_2} \cdot c^{\gamma_3} \cdot d^{\gamma_4} \cdot e^{\gamma_5} \cdot f^{\gamma_6} \cdot g^{\gamma_7} \cdot h^{\gamma_8} \cdot i^{\gamma_9} \cdot j^{\gamma_{10}} \cdot k^{\gamma_{11}} \cdot \theta^{\gamma_{12}} \cdot p^{\gamma_{13}} \cdot E^{-1} \quad (9)$$

where an additional parameter  $p$  is the applied pressure and  $E$  is Young's modulus which is set to  $E = 160$  GPa according to Sharpe et al. (1999) [30].  $N_m$  ( $m = 1, 2$  and  $3$ ) are the coefficients while  $\alpha_n$ ,  $\beta_n$  and  $\gamma_n$  ( $n = 1, 2, \dots, 12$  and  $13$ ) are the exponents. To find the coefficients and exponents of Eq. (7), (8) and (9), one parameter is varied at a time for each case study while the other parameters are kept constant as shown in Table 3. For each case study, five applied pressure values of  $p = 1, 2, 3$ , and  $5$  kPa are tested while case no.1 is used as a reference case.

## 2.4. Piezoresistor Design

The piezoresistor design is crucial for enhancing the performance of the MEMS piezoresistive pressure sensor. In this study, there are three factors that need to be determined in order to improve the sensitivity and the linearity: the placement, the dimension and the configuration of the piezoresistor.

The piezoresistor placement should be located in the area that high longitudinal stress occurs as shown in Fig. 5. Therefore, four piezoresistors are placed in the middle of four beams in this study. The gap between the piezoresistor and the designed layer edge, known as the edge offset as shown in Fig. 6, is optimized to be equal to  $1 \mu\text{m}$ , according to Tran et al. (2018a) [24], in order to achieve the highest sensitivity.

The resistance change in the piezoresistor is dependent on the piezoresistor dimensions, especially the piezoresistor length. The piezoresistor length is properly designed to suit the fabrication technique and to fit the space in the high longitudinal stress zone while the effect of the piezoresistor width is not significant according to Tran et al. (2018a) [24]. In this work, the piezoresistor length and width are  $67 \mu\text{m}$  and  $12 \mu\text{m}$  respectively adopted from Tran et al. (2018a) [24].

The two-turn piezoresistor configuration can enhance the sensitivity and the linearity, according to Tran (2018a) [24]. Therefore, the two-turn configuration is adopted to the proposed piezoresistor as shown in Fig. 6. For p-type silicon, the piezoresistive coefficient  $\pi_{44}$  is dependent on the doping concentration of the material and the temperature [31]. In the present work, the piezoresistors are operated at room temperature (300 K) and the doping concentration of the piezoresistor is  $3 \times 10^{18} \text{ N/cm}^3$  according to Bao (2005) [31] so that, in this study, the piezoresistive coefficient  $\pi_{44}$  is equal to  $138.1 \times 10^{-11} \text{ Pa}^{-1}$ .

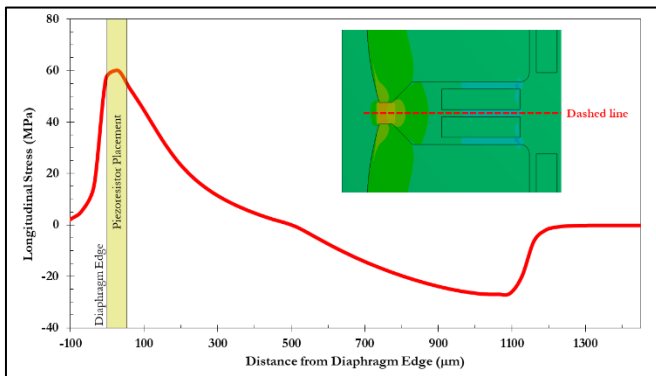


Fig. 5. Distribution of the longitudinal stress along the red dashed line in the proposed MEMS piezoresistive pressure sensor.

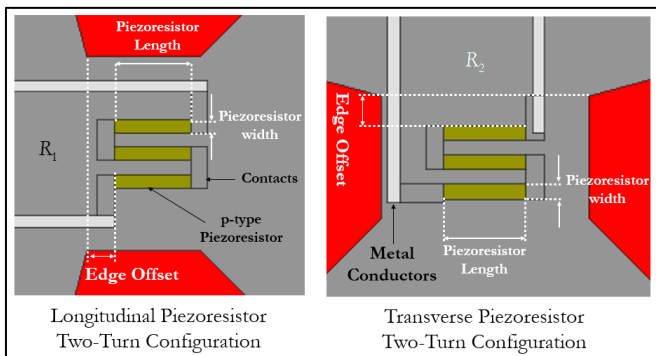


Fig. 6. Details of two-turn piezoresistor configuration. (not to scale)

### 3. Simulation

#### 3.1. Simulation Setup

In this study, FEM is used to find the normal stresses in the longitudinal and transverse directions and also the deflection normal to the diaphragm of the proposed MEMS piezoresistive pressure sensor by using the commercial software ANSYS Mechanical version 18.1. The iterative solver is used for calculation. The bonded contact is specified at the contact surface between two adjacent layers. Due to the symmetry about the center, only one-fourth (top left) part of the mesh distribution of one case study, case study no.1, is shown as an example in Fig. 7. The hexahedral cell type with quadratic element order is generated in all computational domains where the numbers of nodes and elements used for each case study are approximately 1,700,000 and 370,000 respectively. The high-density mesh is generated within the beam region, where the drastic change in the stress occurs, in order to obtain the accurate result. The mesh with at least 4 layers is generated along the heights of both the designed layer and the diaphragm while the mesh with at least 20 layers is required along the height of the center boss.

Figure 8 shows the boundary conditions that are used in the present work. Pressure of 1-5 kPa is applied at the top surfaces of the designed layer and the diaphragm. At the bottom surface, the outer edge of the diaphragm in blue is fixed.

The material properties of silicon used in the simulation are taken from Sharpe et al. (1999) [30]: Young's modulus is 160 GPa and Poisson's ratio is 0.22.

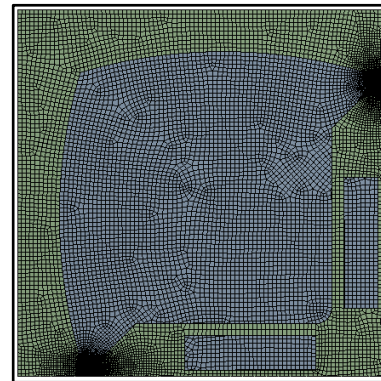


Fig. 7. Mesh distribution of case study no. 1. (Only one fourth of the domain is displayed.)

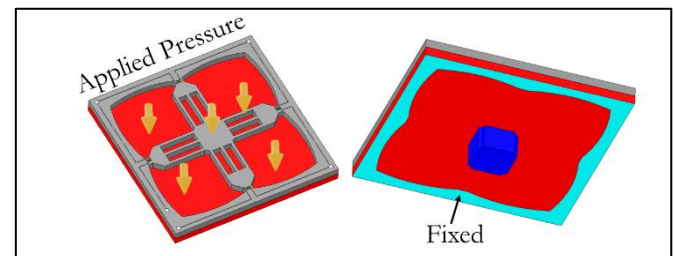


Fig. 8. Boundary conditions for simulation.

#### 3.2. Validation of Simulation

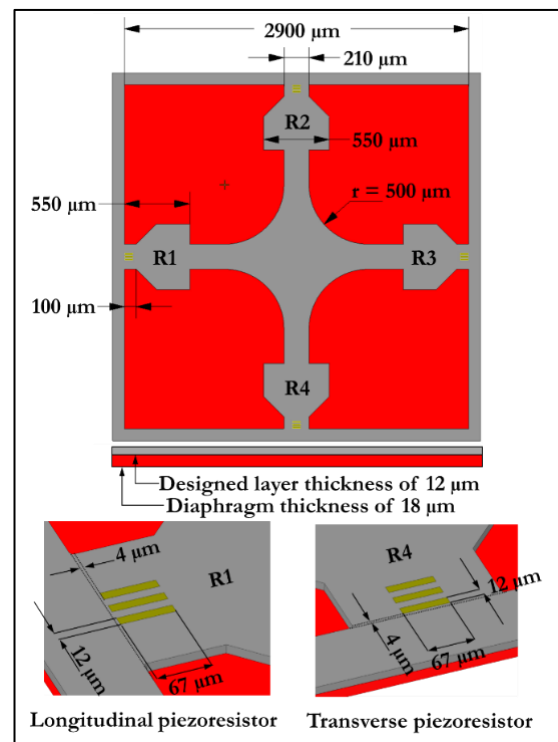


Fig. 9. MEMS piezoresistive pressure sensor of Tran et al. (2018a) [24] used as a validation case.

The MEMS piezoresistive pressure sensor of Tran et al. (2018a) [24] in Fig. 9 is used as a validation case for this

simulation work. Figure 10 shows the mesh distribution of the validation case where the numbers of nodes and elements are 1,705,465 and 360,244 respectively.

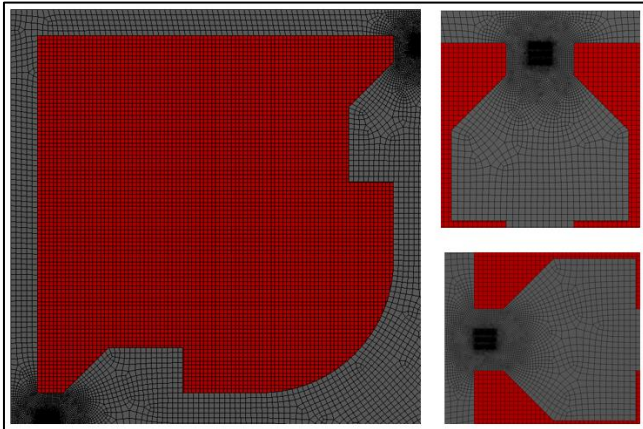


Fig. 10. Mesh distribution of a validation case (Only one fourth of the domain is displayed.)

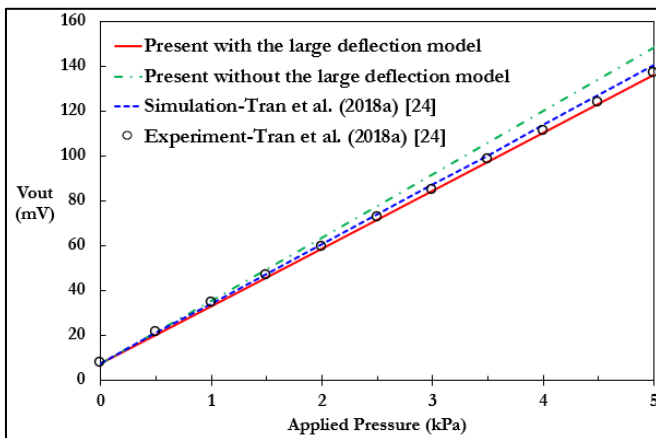


Fig. 11. Comparison of the output voltage.

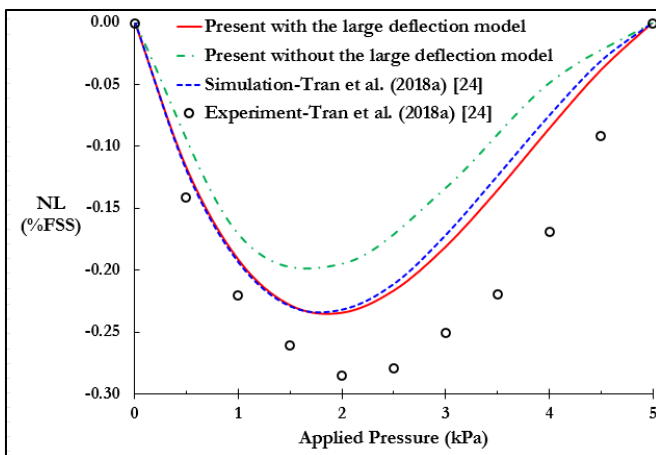


Fig. 12. Comparison of the nonlinearity error.

Under the applied pressure of 0-5 kPa and the input voltage of 5 V, the simulation cases with and without the large deflection model are evaluated in order to find the proper mathematical model to be used for the assessment of the proposed MEMS piezoresistive pressure sensor. To compare the present simulation results with the

experimental data of Tran et al. (2018a) [24], the initial zero output offset of 7.9 mV is specified in the present simulation results. Figures 11 and 12 show the comparisons of the output voltage and the nonlinearity error respectively obtained from the present simulations and the experiment as well as the simulation of Tran et al. (2018a) [24]. The sensitivity of the experimental data is 25.7 mV/kPa while the sensitivity of the present simulation results with and without the large deflection model are 25.74 mV/kPa and 28.23 mV/kPa respectively. The maximum nonlinearity of the experimental data is -0.28% FSS whereas the maximum nonlinearity of the present simulation results with and without the large deflection model are -0.235% FSS and -0.194% FSS respectively. It is obvious that the simulation result with the large deflection model is closer to the experimental data than the one without the large deflection model. Therefore, the large deflection model is employed hereafter in the present study.

## 4. Results and Discussion

### 4.1. Optimal Design of MEMS Piezoresistive Pressure Sensor

The method used to find all the exponents of the geometric parameters in Eq. (7), (8) and (9) is explained here. The exponents of the pedal edge width are determined as an example. Under the applied pressure of 5 kPa, Fig. 13 illustrates the variations of the maximum longitudinal stress ( $\sigma_l$ ), the maximum transverse stress ( $\sigma_t$ ) and the maximum deflection ( $\delta$ ) with the pedal edge width obtained from simulations of case study no. 1, 2, 3 and 4 in Table 3 where only the pedal edge width is varied. Three curves are constructed to fit through three sets of simulation results using the power law in order to find the exponents of the pedal edge width that indicate the influences of the pedal edge width on the maximum longitudinal stress, the maximum transverse stress and the maximum deflection, i.e.  $\alpha_1 = 0.186$ ,  $\beta_1 = 0.239$  and  $\gamma_1 = 0.097$  respectively. The coefficients (27.882, 4.617 and 2.164) are not used.

After all the exponents are determined, 12 geometric parameters with their exponents and the applied pressure are combined to formulate the functional forms for the calculation of  $\phi_{\sigma_l}$ ,  $\phi_{\sigma_t}$  and  $\phi_{\delta}$  as follows:

$$\phi_{\sigma_l} = \frac{a^{0.186} \cdot b^{2.20} \cdot k^{0.009} \cdot \theta^{0.030} \cdot p}{c^{0.017} \cdot d^{0.052} \cdot e^{0.094} \cdot f^{0.213} \cdot g^{0.418} \cdot h^{0.087} \cdot i^{0.414} \cdot j^{2.923}} \quad (10)$$

$$\phi_{\sigma_t} = \frac{a^{0.239} \cdot b^{2.015} \cdot k^{0.012} \cdot \theta^{0.046} \cdot p}{c^{0.015} \cdot d^{0.082} \cdot e^{0.083} \cdot f^{0.198} \cdot g^{0.203} \cdot h^{0.077} \cdot i^{0.485} \cdot j^{2.892}} \quad (11)$$

$$\phi_{\delta} = \frac{a^{0.097} \cdot b^{4.167} \cdot d^{0.057} \cdot k^{0.024} \cdot p}{c^{0.089} \cdot e^{0.050} \cdot f^{0.704} \cdot g^{0.232} \cdot h^{0.135} \cdot i^{0.845} \cdot j^{2.349} \cdot \theta^{0.027}} \quad (12)$$

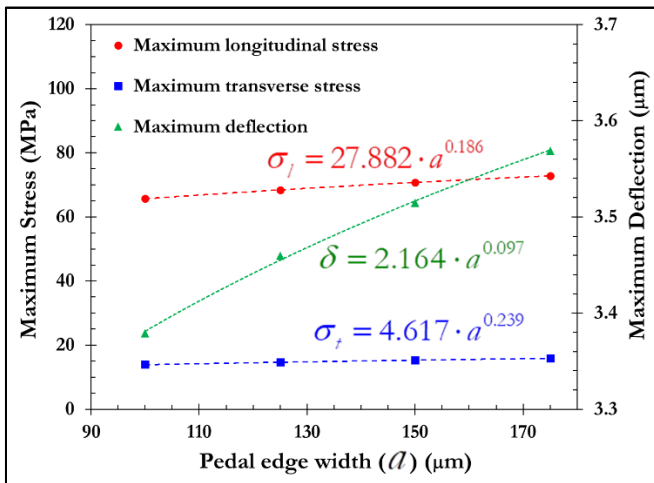


Fig. 13. Variations of the maximum longitudinal stress, the maximum transverse stress and the maximum deflection with the pedal edge width.

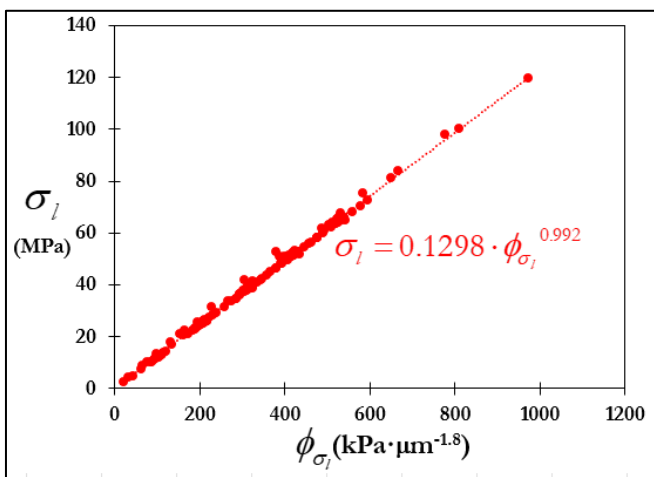


Fig. 14. Variation of the maximum longitudinal stress with 12 geometric parameters and the applied pressure (kPa).

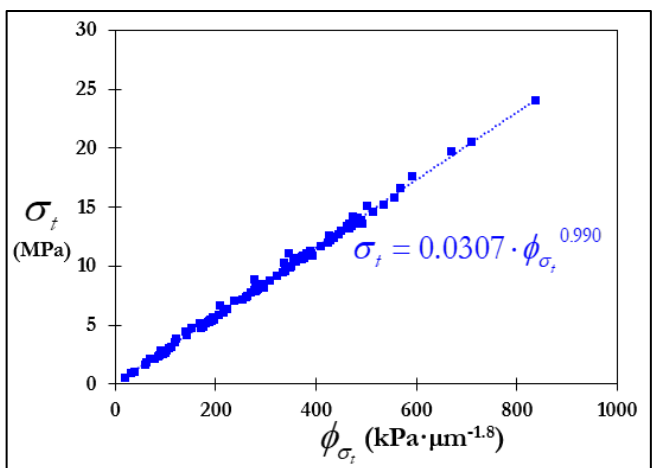


Fig. 15. Variation of the maximum transverse stress with 12 geometric parameters and the applied pressure (kPa).

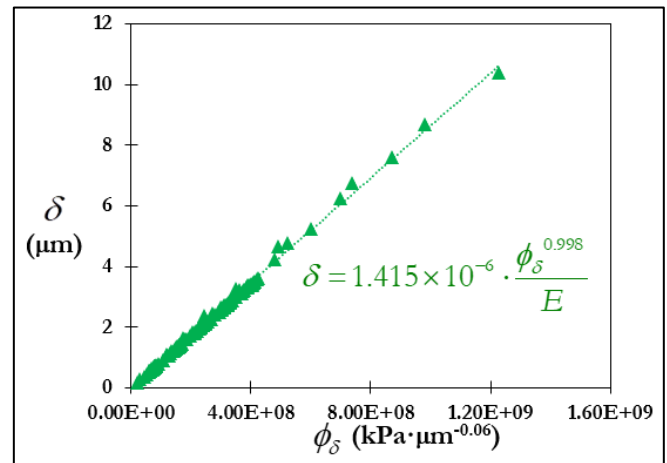


Fig. 16. Variation of the maximum deflection with 12 geometric parameters and the applied pressure (kPa).

To determine the maximum longitudinal stress ( $\sigma_l$ ) in Eq. (7), Eq. (10) is calculated by using all the input data from 36 case studies in Table 3 for the applied pressure of 1-5 kPa. Then, the computed results of the maximum longitudinal stress are plotted versus  $\phi_{\sigma_l}$  as shown in Fig. 14 where there are 180 points. The power law is used to fit through these 180 points in order to obtain the coefficient  $N_1$  of Eq. (7), i.e.  $N_1 = 0.1298$ , and the exponent correction of 0.992 for Eq. (10). For the maximum transverse stress ( $\sigma_t$ ) in Eq. (8) and the maximum deflection ( $\delta$ ) in Eq. (9), Eq. (11) and (12) are used in the same way in order to find  $N_2 = 0.0307$  with the exponent correction of 0.99 for Eq. (11) as shown in Fig. 15 and  $N_3 = 1.415 \times 10^{-6}$  with the exponent correction of 0.998 for Eq. (12) as shown in Fig. 16 respectively. Finally, Eq. (7), (8) and (9) can be formulated in the functional forms as follows:

$$\sigma_l = 0.1298 \left( \frac{a^{0.184} \cdot b^{2.187} \cdot k^{0.009} \cdot \theta^{0.030} \cdot p^{0.992}}{c^{0.017} \cdot d^{0.052} \cdot e^{0.093} \cdot f^{0.211} \cdot g^{0.414} \cdot h^{0.087} \cdot i^{0.410} \cdot j^{2.901}} \right) \quad (13)$$

$$\sigma_t = 0.0307 \left( \frac{a^{0.237} \cdot b^{1.995} \cdot k^{0.011} \cdot \theta^{0.046} \cdot p^{0.990}}{c^{0.015} \cdot d^{0.081} \cdot e^{0.082} \cdot f^{0.1959} \cdot g^{0.201} \cdot h^{0.076} \cdot i^{0.481} \cdot j^{2.864}} \right) \quad (14)$$

$$\delta = 1.415 \times 10^{-6} \left( \frac{a^{0.097} \cdot b^{4.161} \cdot d^{0.057} \cdot k^{0.024} \cdot p^{0.998}}{e^{0.089} \cdot f^{0.050} \cdot g^{0.703} \cdot h^{0.231} \cdot i^{0.135} \cdot j^{0.844} \cdot k^{2.345} \cdot \theta^{0.027} \cdot E} \right) \quad (15)$$

where the unit of longitudinal and transverse stresses is MPa, the unit of deflection is  $\mu\text{m}$ , the unit of the geometric parameters is  $\mu\text{m}$ , the unit of the angle ( $\theta$ ) is degree, the unit of the applied pressure is kPa and the unit of Young's modulus is GPa.

The R squared ( $R^2$ ) is calculated to measure the accuracy of Eq. (13), (14) and (15), where  $R^2$  of  $\sigma_l$ ,  $\sigma_t$  and  $\delta$  are all equal to 0.998. However, Eq. (13) and (14)

underpredict  $\sigma_l$  and  $\sigma_t$  when the diaphragm thickness is larger than 20  $\mu\text{m}$ . Eq. (13), (14) and (15) later are used to design the optimal MEMS piezoresistive pressure sensor proposed in this work. Since the MEMS piezoresistive pressure sensor proposed in this work is developed further from that of Tran et al. (2018b) [25], the key geometric parameters such as the diaphragm width ( $b$ ), the designed layer thickness ( $i$ ) and the diaphragm thickness ( $j$ ) are specified following Tran et al. (2018b) [25], i.e.  $b = 2900 \mu\text{m}$ ,  $i = 12 \mu\text{m}$  and  $j = 16 \mu\text{m}$ . In Eq. (13), (14) and (15), besides the aforementioned key geometric parameters, the maximum longitudinal stress, the maximum transverse stress and the maximum deflection are highly dependent on the petal edge width ( $a$ ), the center boss width ( $f$ ), the beam width ( $g$ ) and the cross beam width ( $h$ ) while the other geometric parameters have very little effect. Therefore, only four geometric parameters, i.e.  $a$ ,  $f$ ,  $g$  and  $h$ , are optimized while the other geometric parameters are fixed as specified in the case study no. 1 in Table 3.

Figure 17 shows the maximum deflection versus the maximum stress difference under the applied pressure of 5 kPa evaluated by Eq. (13), (14) and (15) for 256 case studies. The optimal design is selected based on two conditions: 1) the case studies qualified within the design region in Fig. 17 give the maximum deflection less than 20% of the diaphragm thickness, according to the condition of Timoshenko (1989) [32], in order to maintain the linearity of the MEMS piezoresistive pressure sensor. 2) within the design region in Fig. 17, the case study that gives the highest value for the maximum stress difference is chosen as the optimal design in order to achieve highest sensitivity for the MEMS piezoresistive pressure sensor.

As a result, four geometric parameters optimized are  $a = 175 \mu\text{m}$ ,  $f = 810 \mu\text{m}$ ,  $g = 170 \mu\text{m}$  and  $h = 57 \mu\text{m}$ . Therefore, the geometric parameters of the optimal design of the proposed MEMS piezoresistive pressure sensor can be summarized in Table 4.

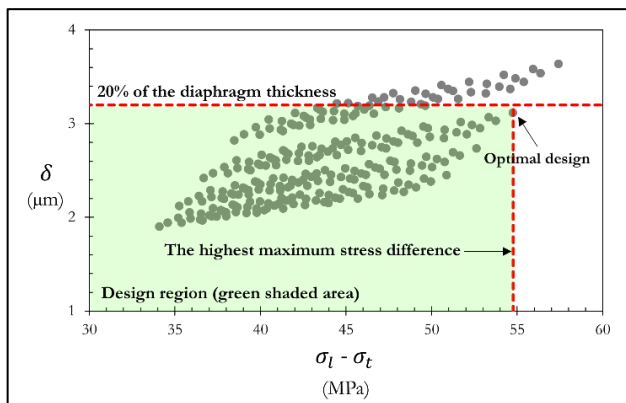


Fig. 17. Maximum deflection versus maximum stress difference under the applied pressure of 5 kPa for 256 case studies.

Table 4. Geometric parameters of the optimal design of the proposed MEMS piezoresistive pressure sensor.

Parameter	value
$a$ ( $\mu\text{m}$ )	175
$b$ ( $\mu\text{m}$ )	2900
$c$ ( $\mu\text{m}$ )	500
$d$ ( $\mu\text{m}$ )	100
$e$ ( $\mu\text{m}$ )	400
$f$ ( $\mu\text{m}$ )	810
$g$ ( $\mu\text{m}$ )	170
$h$ ( $\mu\text{m}$ )	57
$i$ ( $\mu\text{m}$ )	12
$j$ ( $\mu\text{m}$ )	16
$k$ ( $\mu\text{m}$ )	200
$\theta$ (degree)	45

#### 4.2. Performance of the Present Design

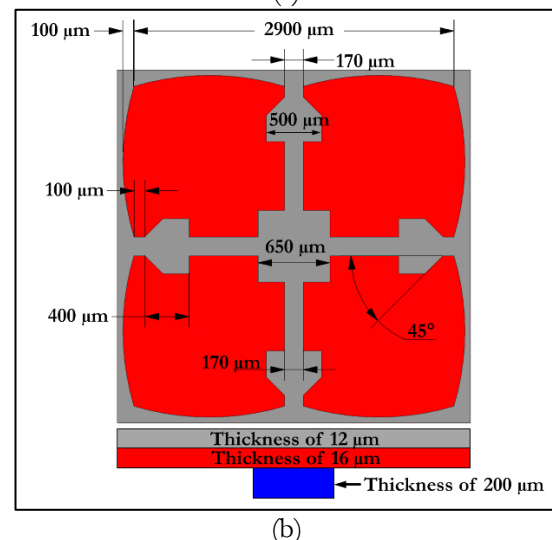
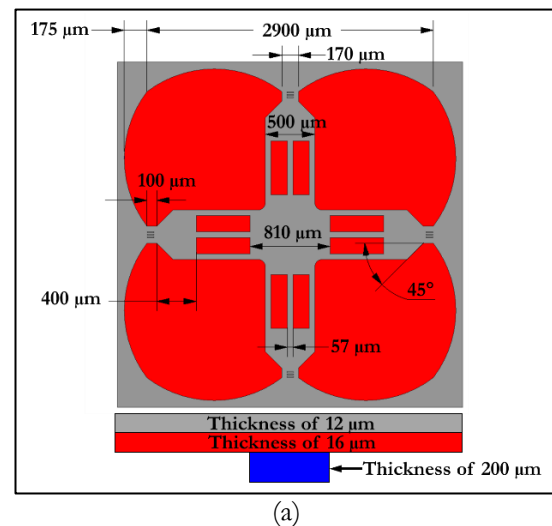


Fig. 18. Dimensions of the MEMS piezoresistive pressure sensors: (a) the proposed design and (b) the design by Tran et al. (2018b) [25] (not to scale).

The optimal design of the MEMS piezoresistive pressure sensor in the present work is compared to that of Tran et al. (2018b) [25] in Fig. 18. In order to evaluate the sensor performance, FEM is used to calculate the stress and the deflection of these MEMS piezoresistive pressure sensors. Figure 19 shows the equivalent stress distribution under the applied pressure of 5 kPa on the piezoresistor placement areas of the proposed MEMS piezoresistive pressure sensor where the equivalent stress of the proposed MEMS piezoresistive pressure sensor is higher than that of Trans et al. (2018b) [25]. Figure 20 shows the comparison of the longitudinal stress and the transverse stress between the MEMS piezoresistive pressure sensor of the present work and that of Tran et al. (2018b) [25] where the longitudinal stress and the transverse stress of the proposed design are found to be higher.

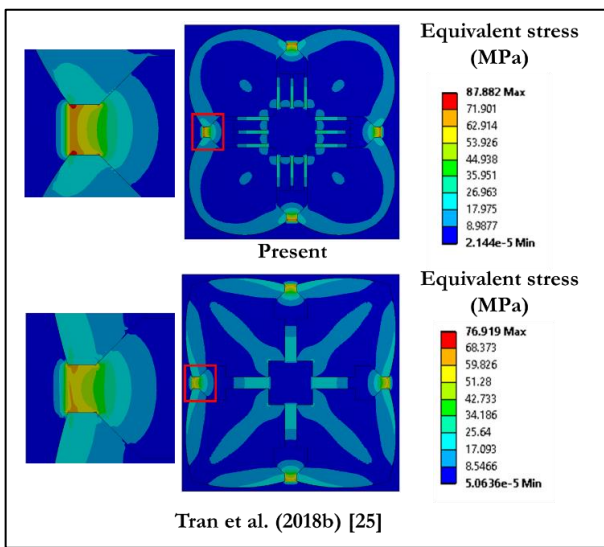


Fig. 19. Simulation results of the equivalent stress distribution under the applied pressure of 5 kPa on the MEMS piezoresistive pressure sensor.

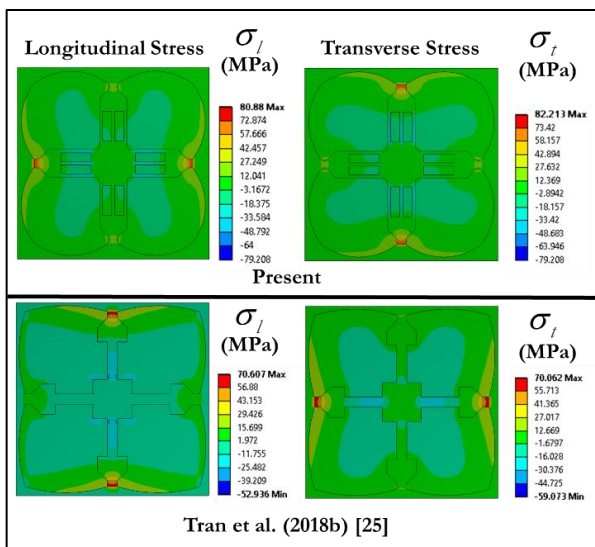


Fig. 20. Simulation results of the longitudinal and transverse stresses under the applied pressure of 5 kPa on the MEMS piezoresistive pressure sensor.

Figure 21 clearly shows that the present design can induce the longitudinal stress and the transverse stress in the piezoresistors placement area higher than that of Tran et al (2018b) [25]. Therefore, the sensitivity of the proposed design is increased.

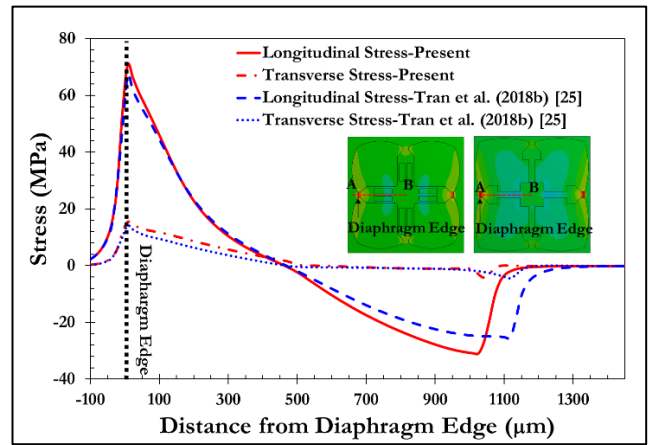


Fig. 21. Distributions of the longitudinal stress and the transverse stress along the line AB under the applied pressure of 5 kPa.

Figure 22 shows the simulation results of the stress difference between the longitudinal stress and the transverse stress ( $\sigma_l - \sigma_t$ ) on the piezoresistors when subjected to the applied pressure of 5 kPa. It is found that the averaged stress difference on the piezoresistors of the proposed design is significantly higher than that of Trans et al. (2018b) [25] as summarized in Table 5.

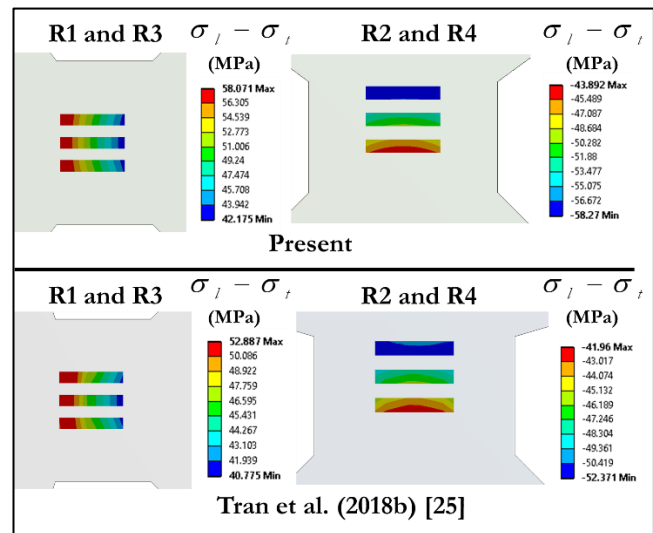


Fig. 22. Distribution of stress difference between the longitudinal stress and the transverse stress ( $\sigma_l - \sigma_t$ ) on the piezoresistors under the applied pressure of 5 kPa.

For the input voltage of 5 V the averaged stress difference of the longitudinal piezoresistor and the transverse piezoresistor are used in Eq. (6) to calculate  $\Delta R_1 / R_1$  and  $\Delta R_2 / R_2$  respectively. Therefore, the

output voltage can be determined by Eq. (5) and the sensitivity and the nonlinearity error are calculated by Eq. (3) and (4) respectively.

Table 5. Averaged stress difference of the longitudinal piezoresistor and the transverse piezoresistor under the applied pressure of 5 kPa.

Averaged stress difference	Present design (MPa)	Tran et al. (2018b) [25] (MPa)	% Increase in averaged stress difference
$R_1$ and $R_3$	48.98	42.9	14.17
$R_2$ and $R_4$	-49.69	-42.39	-17.22

Under the applied pressure of 0-5 kPa and the input voltage of 5 V, Fig. 23 shows the variation of the output voltage versus the applied pressure of the proposed MEMS piezoresistive pressure sensor compared to that of Tran et al. (2018b) [25]. The result shows that the sensitivity of the proposed MEMS piezoresistive pressure sensor, i.e. 34 mV/kPa, is 14.7% higher than that of Tran et al. (2018b) [25], i.e. 29 mV/kPa.

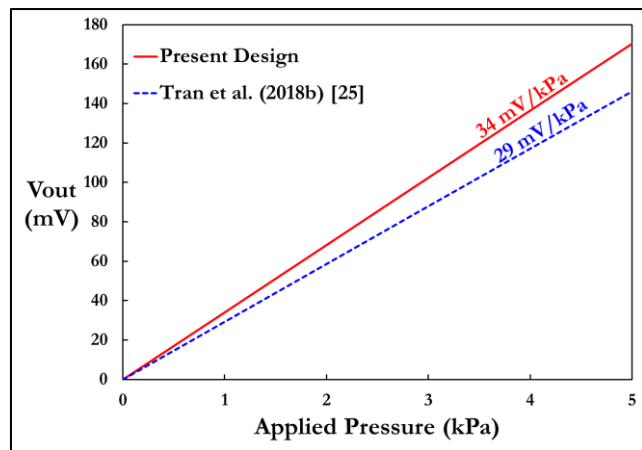


Fig. 23. Variation of the output voltage versus the applied pressure and the input voltage of 5 V.

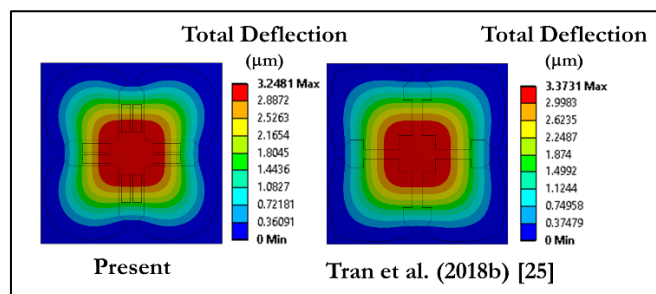


Fig. 24. Simulation results of the total deflection of the MEMS piezoresistive pressure sensor under the applied pressure of 5 kPa.

The total deflection of the diaphragm can be used to determine the linearity of the sensor where the small

deflection can help maintain the linearity of the sensor. Figures 24 and 25 clearly show that, under the applied pressure of 5 kPa, the present design can reduce the maximum deflection at the center of the diaphragm much more than that of Tran et al. (2018b) [25] so that the nonlinearity error of the present design can maintain a low nonlinearity error of 0.11% FSS which is 41.8% lower than that of Tran et al. (2018b) [25], i.e. 0.19% FSS, as shown in Fig. 26.

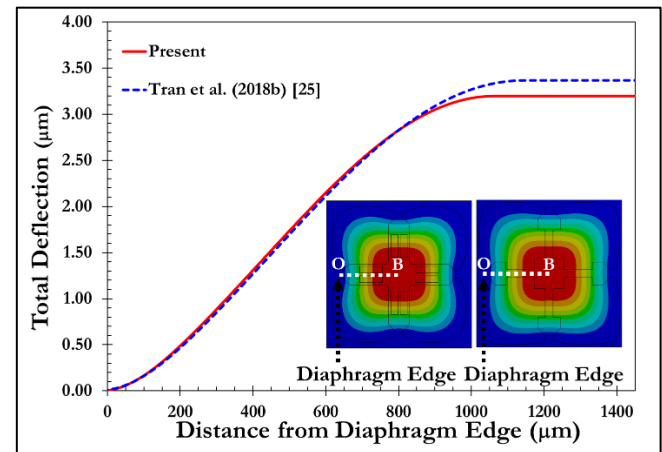


Fig. 25. Distributions of the total deflection along the line OB under the applied pressure of 5 kPa.

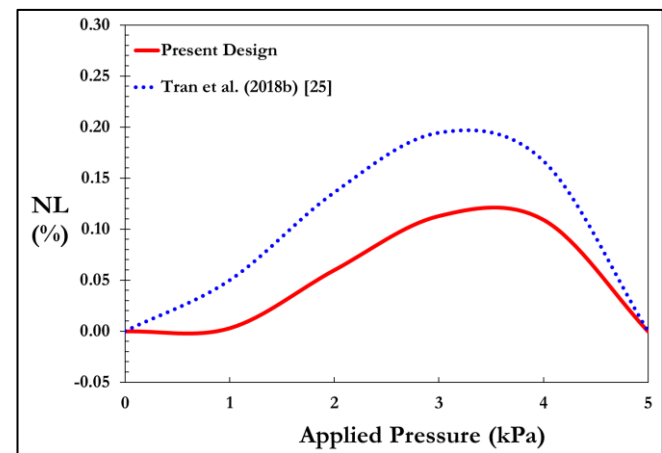


Fig. 26. Variation of the nonlinearity error versus the applied pressure and the input voltage of 5 V.

For this design of the MEMS piezoresistive pressure sensor, three cross beams and the new dimension of the center boss width proposed here can reduce the maximum deflection. Therefore, the linearity is improved, compared to design of Tran et al. (2018b) [25]. For the sensitivity improvement, the petal edge width is intended to be increased from that of Tran et al. (2018b) [25], i.e. from 100  $\mu\text{m}$  to 175  $\mu\text{m}$ , in order to increase the stress at the piezoresistor placement area and hence the increase in the sensitivity.

## 5. Conclusions

The MEMS piezoresistive pressure sensor of Tran et al. (2018b) [25] is improved in this work. FEM is used to calculate the stress and the deflection of the MEMS piezoresistive pressure sensor under the applied pressure of 1-5 kPa. The relations of the maximum longitudinal stress, the maximum transverse stress and the maximum deflection with twelve geometric parameters are formulated using the power law. The maximum longitudinal stress, the maximum transverse stress and the maximum deflection are strongly dependent on six geometric parameters: the petal edge width ( $a$ ), the diaphragm width ( $b$ ), the center boss width ( $f$ ), the beam width ( $g$ ), the design layer thickness ( $i$ ) and the diaphragm thickness ( $j$ ). The cross beam width ( $h$ ) significantly affects the maximum deflection only. The simulation results show that, compared to Tran et al. (2018b) [25], the sensitivity of the optimal design of the proposed MEMS piezoresistive pressure sensor is increased up to 14.7% while its nonlinearity error is reduced to 41.8%. However, the proposed MEMS piezoresistive pressure sensor is studied at room temperature (300 K). Therefore, the sensitivity and linearity may be reduced when the proposed sensor is used at higher temperature environment. The temperature sensitivity can be reduced by using the base resistance of a MOSFET as the piezoresistor in the Wheatstone bridge circuit. For further development of the present MEMS piezoresistive pressure sensor, a groove along the diaphragm edge is of future interest.

## Acknowledgement

The first author (PT) is financially supported by the Thailand Graduate Institute of Science and Technology (TGIST) scholarship of National Science and Technology Development Agency (NSTDA) and the tuition-fee-waiving scholarship from the Sirindhorn International Thai-German Graduate School of Engineering (TGGGS), King Mongkut's University of Technology North Bangkok (KMUTNB).

## References

- [1] W. P. Eaton and J. H. Smith, "Micromachined pressure sensors review and recent developments," *Smart Material and Structure*, vol. 6, no. 5, pp. 530-539, 1997.
- [2] R. Bogue, "Recent developments in MEMS sensors: A review of applications, markets and technologies," *Sensor Review*, vol. 33, no. 4, pp. 300-304, 2013.
- [3] S. S. Kumar and B. D. Pant, "Design principles and considerations for the 'ideal' silicon piezoresistive pressure sensor: A focused review," *Microsystem Technologies*, vol. 20, pp. 1213-1247, 2014.
- [4] B. Tian, Y. Zhao, and Z. Jiang, "The novel structure design for pressure sensors," *Sensor Review*, vol. 30, no. 4, pp. 305-313, 2010.
- [5] T. Ishikawa, T. Odohira, M. Nikkuni, E. Koyama, T. Tsumagari, and R. Asada, "New DPharp EJX series pressure and differential pressure transmitters," *Yokagawa Technical Report*, no. 37, pp. 9-14, 2004.
- [6] C. J. Welham, J. Greenwood and M. M. Bertoli, "A high accuracy resonant pressure sensor by fusion bounding and trench etching," *Sensors and Actuators*, vol. 76, pp. 298-304, 1999.
- [7] E. Vorathin, Z. M. Hafizi, N. Ismail, and M. Loman, "Review of high sensitivity fibre-optic pressure sensors for low pressure sensing," *Optics and Laser Technology*, vol. 121, no. 5, pp. 530-539, 1997.
- [8] Z. Niu, Y. Zhao, and B. Tian, "Design optimization of high pressure and high temperature piezoresistive pressure sensor for high sensitivity," *Review of Scientific Instruments*, vol. 85, 2014.
- [9] K. J. Suja, G. S. Kumar, A. Nisanth, and R. Komaragiri, "Dimension and doping concentration based noise and performance optimization of a piezoresistive MEMS pressure sensor," *Microsystem Technologies*, vol. 21, pp. 831-839, 2015.
- [10] C. Li, F. Cordovilla, R. Jagdheesh, and J. L. Ocaña, "Design and optimization of a novel structure MEMS piezoresistive pressure sensor," *Microsystem Technologies*, vol. 23, pp. 4531-4541, 2017.
- [11] A. A. Barlian, W. T. Park, J. R. Mallon, A. J. Rastegar, and B. L. Pruitt, "Review: Semiconductor piezoresistance for microsystem," in *Proceeding of the IEEE*, 2009, vol. 97, no. 3, pp.513-552.
- [12] D. Sparks, "MEMS pressure and flow sensors for automotive engine management and aerospace applications," in *MEMS for Automotive and Aerospace Application*. Woodhead Publishing Limited, 2013, ch. 4, sec. 1, pp. 78-105.
- [13] P. Wadhvani and S. Yadav. "Pressure sensor market size." GMInsights. <http://www.gminsights.com/industry-analysis/pressure-sensor-market> (accessed 15 December 2021)
- [14] D. Dimitrio and M. Jérôme, "MEMS pressure sensors – Technology and market trend 2021," Yole Development: Market and Technology Report, 2021.
- [15] L. Li, N. Belov, M. Klitzke, and J-S. Park, "High performance piezoresistive low pressure sensors," *2016 IEEE Sensors*, pp. 1-3, 2016.
- [16] H. P. Phan, K. M. Dowling, T. K. Nguyen, T. Dinh, D. G. Senesky, T. Namazu, D. V. Dao, and N. T. Nguyen, "Highly sensitive pressure sensors employing 3C-SiC nanowires fabricated on a free standing structure," *Materials and Design*, vol. 156, pp. 16-21, 2018.
- [17] H. P. Phan, Y. Zhong, T.K. Nguyen, Y. Park, T. K. Dinh, E. Song, R. K. Vadivelu, M. K. Masud, J. Li, M. J. A. Shiddiky, D. V. Dao, Y. Yamauchi, J. A. Rogers, and N. T. Nguyen, "Long-lived, transferred crystalline silicon carbide nanomembranes for

- Implantable flexible electronics,” *ACS Nano*, vol. 13, no. 10, pp. 11572-11581, 2019.
- [18] M. Basov, “Pressure sensor with novel electrical circuit utilizing bipolar junction transistor,” in *2021 IEEE Sensors.*, Sydney, Australia, 2021, pp. 1-4.
- [19] N. Hafez, S. Haas, K. U. Loebel, D. Reuter, M. Ramsbeck, M. Schramm, J. T. Horstmann, and T. Otto, “Characterisation of MOS transistors as an electromechanical transducer for stress,” *Phys. Status Solidi A*, vol. 216, p. 1700680, 2019.
- [20] H. Sandmaier and K. Kuhl, “A square-diaphragm piezoresistive pressure sensor with a rectangular central boss for low-pressure ranges,” *Transactions on Electron Devices*, vol. 40, no. 10, Oct. 1993.
- [21] X. Huang and D. Zhang, “A high sensitivity and high linearity pressure sensor based on a peninsula-structured diaphragm for low-pressure ranges,” *Sensors and Actuators A*, vol. 216, pp. 176-189, Sep. 2014.
- [22] T. Guan, F. Yang, W. Wang, X. Huang, B. Jiang, and D. Zhang, “The design and analysis of piezoresistive shuriken-structured diaphragm micro-pressure sensors,” *Journal of Microelectromechanical Systems*, vol. 26, no. 1, Feb. 2017.
- [23] B. Zhu, X. Zhang, Y. Zhang, and S. Fatikow, “Design of diaphragm structure for piezoresistive pressure sensor using topology optimization,” *Structural and Multidisciplinary Optimization*, vol. 55, pp. 317-329, 2017.
- [24] A. V. Tran, X. Zhang, and B. Zhu, “The development of a new piezoresistive pressure sensor for low pressure,” *Transactions on Industrial Electronics*, vol. 65, no. 8, pp. 6487-6496, Aug. 2018.
- [25] A. V. Tran, X. Zhang, and B. Zhu, “Mechanical structural design of a piezoresistive pressure sensor for low-pressure measurement: A computational analysis by increases in the sensor sensitivity,” *Sensors*, vol. 18, no. 7, 2018.
- [26] M. Basov, “Development of high-sensitivity pressure sensor with on-chip differential transistor amplifier,” *Journal of Micromechanics and Microengineering*, vol. 30, no. 6, 2020.
- [27] G. K. Johns, “Modeling piezoresistivity in silicon and polysilicon,” *Journal of Applied Engineering Mathematics*, vol. 2, Apr. 2006.
- [28] M. Messina, J. Njuguna, and C. Palas, “Mechanical structure design of a MEMS-based piezoresistive accelerometer for head injuries monitoring: A computational analysis by increments of the sensor mass moment of inertia,” *Sensors*, vol. 18, no. 1, 2018.
- [29] Y. Kanda, “A graphical representation of the piezoresistance coefficients in silicon,” *IEEE Transactions on Electron Devices*, vol. 29, no. 1, pp. 64-70, Jan. 1982.
- [30] W. N. Sharpe, K. T. Turner, and R. L. Edwards, “Tensile testing of polysilicon,” *Experimental Mechanics*, vol. 39, no. 3, pp. 162-170, Sep. 1999.
- [31] M. Bao, “Piezoresistive sensing,” in *Analysis and Design Principles of MEMS Devices*. Amsterdam, The Netherlands, 2005, ch. 6, sec. 1, pp. 247-254.
- [32] S. Timoshenko, “Large deflections of plates,” in *Theory of Plates and Shells*. McGraw-Hill Book Company, 1989, ch. 13, pp. 396-428.

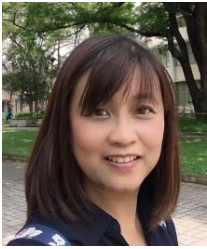


**Phongsakorn Thawornsathit** received B.Eng. degree in mechanical engineering from Kasetsart University Sriracha Campus (KU SRC), Thailand, in 2014. He started working as Building Information Modeling (BIM) engineer at Jardine Engineering Corporation (JEC), Bangkok, Thailand, in 2014. In 2015, he was an inspection engineer at PTT Maintenance and Engineering (PTTME), Rayong, Thailand. In 2017, he pursued M.Eng. degree in mechanical engineering at Kasetsart University (KU), Thailand. During his Master degree, he receives the research assistant scholarship from Faculty of Engineering, KU. Since 2019, he has been a Ph.D. candidate in Mechanical Engineering Simulation and Design (MESD) group at The Sirindhorn International Thai-German Graduate School of Technology (TGGS), King Mongkut’s University of Technology North Bangkok (KMUTNB), Thailand. He receives the Thailand Graduate Institute of Science and Technology (TGIST) scholarship of National Science and Technology Development Agency (NSTDA), during his doctoral study. His research interests are MEMS piezoresistive pressure sensor, transition and turbulence modelling and turbomachinery flow in power plants.



**Ekachai Juntasaro** received B.Eng. degree in mechanical engineering from King Mongkut’s Institute of Technology Ladkrabang (KMITL), Thailand, in 1989, and pursued both M.Sc. and Ph.D. degrees in mechanical engineering at Imperial College London, U.K., in 1992 and 1997 respectively with the Royal Thai Government Scholarship. In 1997, he started working as Lecturer at School of Mechanical Engineering, Institute of Engineering, Suranaree University of Technology (SUT), Nakhon Ratchasima, Thailand, where he became Assistant Professor and Associate Professor in 2001 and 2006 respectively. Since 2008, he has worked as Associate Professor in Mechanical Engineering Simulation and Design (MESD) Group at The Sirindhorn International Thai-German Graduate School of Technology (TGGS), King Mongkut’s University of Technology North Bangkok (KMUTNB),

Thailand. His research interests are transition and turbulence modelling with/without analytical wall function (AWF), unstructured finite volume method for computational fluid dynamics (CFD), microfluidics, and turbomachinery flow in power plants.



**Hwanjit Rattanasonti** graduated with her M.S. in Electrical Engineering (2003) from the San José State University (California, USA). She received her Ph.D. (2015) in Electronics and Computer Science from the University of Southampton (UK). She has held positions as Research Staff at Thai Microelectronics Center (TMEC) as part of National Electronic and Computer Technology Center (NECTEC), Thailand since 2015. Her research's works have been developed in the areas of Energy Harvesting, MEMS and sensors, all with design, simulation, fabrication and experimental activities. In 2018, she also held a position on MEMS Research Team Lead, focusing on the MEMS fabrication technologies and devices such as MEMS pressure sensor, microphone and gyroscope.



**Putapon Pengpad** received B.Sc degree in physics from Chiang Mai University, Thailand, and M.Sc and Ph.D. degrees in electronics and computer science from University of Southampton, UK in 1998, 2002 and 2008 respectively. His research is emphasized on design, simulation, fabrication and characterization of semiconductor device based on bipolar and heterojunction bipolar technology on integrated circuit. He is currently working at Thai Microelectronic Center (TMEC) as part of National Electronic and Computer Technology Center (NECTEC), Thailand, and focuses on smart sensor project, microfabrication technology and MEMS device.



**Karoon Saejok** received B.Sc degree in Physics from Prince of Songkla University in 1996 and M.Eng. degree from King Mongkut's Institute of Technology, Ladkrabang, Thailand in 2007. He worked at Submicron Technology PLC from 1996 to 1998 as a process engineer. Then he moved to Hypoelectronics PLC as a project engineer in assembly plant from 1998-2000. Since then he has worked as a researcher at Thai Microelectronics Center (TMEC) under the National Science and Technology Development Agency (NSTDA), Thailand. His research interests are MEMS piezoresistive pressure sensor device and Si sensor device fabrication.



**Chana Leepattarapongpan** received B.S. and M.S. degrees in microelectronic engineering, and Ph.D. degree in electrical engineering from King Mongkut's Institute of Technology Ladkrabang, Thailand, in 2003, 2006 and 2016 respectively, He has been researcher at Thai Microelectronic Center (TMEC), National Electronics and Computer Technology Center (NECTEC), since 2007. His major research areas are microfabrication technology, thin film technology, magnetic sensor device and MEMS device.



**Ekalak Chaowicharat** is a researcher at Thai Microelectronics Center (TMEC). He was a Royal Thai Government Scholarship student. He received B.Eng. degree in electrical engineering from the University of New South Wales, Sydney, Australia. His day-to-day duty involves process integration of MEMS devices as well as other cleanroom related processes such as LPCVD. In addition, he also offers technical advisory and management for various projects both internal and external works. His interests include but not limit to Microfabrication technologies, Microelectromechanical System (MEMS), Microelectronics as well as VLSI design.



**Wutthinan Jeamsaksiri** was born in Bangkok, Thailand in 1974. He received his M.Eng. and Ph.D. from Department of Electrical and Electronic Engineering, Imperial College, London in 1996 and 2003, respectively. He then worked as a process integration engineer on a European project at IMEC, Leuven, Belgium from 2000 to 2004. The project then was on Integration of Microwave Performance Advanced CMOS Technology. From 2005, he has been working at Thai Microelectronics Center (TMEC) under the National Electronics and Computer Technology Center (NECTEC). In 2018 he took the position as the director of TMEC. His work interest includes Si based sensors, MEMS, microfluidic devices: Lab on Chip (LOC) and Lab On A Disc (LOAD), and Surface texturing and modification for various applications.